THE PENNSYLVANIA STATE UNIVERSITY
SCHREYER HONORS COLLEGE

DEPARTMENT OF CHEMICAL ENGINEERING

AMMONIA ELECTRO-OXIDATION MECHANSIM ON THE PLATINUM (100) SURFACE

SPENCER WALLACE
SPRING 2019

A thesis
submitted in partial fulfillment
of the requirements
for a baccalaureate degree
in Chemical Engineering
with honors in Chemical Engineering

Reviewed and approved* by the following:

Michael Janik
Professor of Chemical Engineering
Thesis Supervisor and Honors Adviser

Xueyi Zhang
Assistant Professor of Chemical Engineering
Faculty Reader

* Signatures are on file in the Schreyer Honors College.

ABSTRACT

The catalytic electrochemical oxidation of ammonia is a structure-sensitive reaction that will potentially play a role in future energy systems, including portable fuel cells and the elimination of harmful pollutants. Platinum is an ideal catalyst for this reaction because of its selectivity toward the formation of nitrogen gas. The Pt (100) facet shows much faster ammonia electroxidation than other facets of Pt, however the elementary reaction steps responsible for this phenomenon are not understood. Density functional theory (DFT) calculations are used to determine elementary reaction thermodynamics and kinetics. Absorbed NH_2* formation is rapid and this intermediate is very stable on Pt (100). High coverage NH_2* binds at atop sites, enabling favorable N-N bond formation. The faster rate of ammonia oxidation on Pt (100) results from the low barrier of N_2H_4* formation resulting from NH_2* dimerization at high coverage. Understanding the reactivity of ammonia oxidation of Pt (100) can aid in electrochemical reaction mechanism development and catalyst design.

TABLE OF CONTENTS

LIST OF FIGURES

LIST OF TABLES

ACKNOWLEDGEMENTS

Chapter 1

Introduction

Ammonia is one of the most widely produced chemicals; its production alone consumes approximately 1.5% of the world's energy supply.[1] It is used mainly as an industrial feedstock to produce a variety of nitrogen containing compounds, and either directly as a fertilizer or as a feedstock for fertilizer synthesis, where it is responsible for supporting food production for half of the world population.[2,3] The extended use of ammonia as a fertilizer has caused it to be a very common water pollutant in continental waters as well as in industrial wastewater.[4,5] In addition, hydrogen carrying molecules, like ammonia, can be used to generate power in electrochemical fuel cells as a more energy dense alternative to hydrogen.[6] Therefore, electrochemical ammonia oxidation is an important reaction that can be involved in the elimination of harmful pollutants and generation of sustainable power in portable fuel cells.

The catalytic electrochemical oxidation of ammonia is a structure-sensitive reaction that produces electrons at the anode of an ammonia fuel cell. Electrochemical oxidation nullifies the necessity of a synthetic oxidizer, meaning air can be used. Platinum is an ideal catalyst for electrocatalytic oxidation of ammonia because of its relatively fast rate and selectivity toward the formation of N_2 gas.[7, 8] The rate of ammonia oxidation on the Pt (100) surface is much faster than other facets of Pt as demonstrated with thermal desorption spectrometry and kinetic studies of preferentially oriented nanoparticles.[9, 31, 32] The elementary reaction mechanisms responsible for the higher rate on Pt (100) facets are not understood at the molecular level. Rosca and Koper showed that Tafel slopes on the Pt (100) surface suggest the rate determining step is a chemical

step following two electrochemical steps, while Tafel slopes on Pt (111) suggest two electrochemical steps, with the latter being rate determining.[10] Understanding the reactivity of ammonia oxidation on the Pt (100) surface will help in designing a more economical catalyst with similar efficiency, and aid in our broader understanding of electrochemical reaction mechanisms.[11, 12] We use density functional theory (DFT) to investigate the NH_3 electroxidation mechanism on the Pt (100) surface, with comparison to literature data for the Pt (111) surface.

Density functional theory can be used to model ammonia oxidation on the molecular (atomistic) level. DFT can describe the most active path of ammonia oxidation on Pt (100) and Pt (111), enabling the calculation of elementary oxidation step thermodynamics and kinetics (activation energies) for each facet. Mavrikakis et al. described electrochemical oxidation of ammonia on Pt (111) using DFT; our Pt (100) data will be compared to their reported energetics throughout this paper.[13] Katsounaros et al. used both experiment and DFT to examine ammonia oxidation specifically on Pt (100), however, they did not examine the coverage dependence in the adsorption of reaction intermediates and activation energies.[14] We will compare our coverage dependent results with their calculations at the low coverage limit.

The Gerischer and Mauerer mechanism, proposed in 1970, is the most accepted ammonia oxidation mechanism.[33] This mechanism is outlined in Scheme 1, in which NH_3* is deprotonated by hydroxyl ions in the first three steps to release electrons and form water molecules. Adsorbed NH_x* and NH_y* species bind together to form N-N bonds, creating H_xNNH_y* species. N_2 is formed through deprotonation of these species, resulting in the desorption of N_2 from the surface. The two paths considered are the Gerischer and Mauerer mechanism and a mechanism involving N-N bond formation through N adatoms, denoted as the "N+N mechanism".

Scheme 1: Gerischer and Mauerer mechanism, where * denotes a surface site or adsorbed species.

$$NH_3 + OH^- + * \rightarrow NH_2* + H_2O + e^-$$

$$NH_2* + OH^- + * \rightarrow NH* + H_2O + e^-$$

$$NH* + OH^- + * \rightarrow N* + H_2O + e^-$$

$$NH_x* + NH_y* \rightarrow H_xNN_y* + *$$

$$H_xNNH_y* + (x+y) OH^- \rightarrow N_2 + (x+y)H_2O + (x+y)e^- + *$$
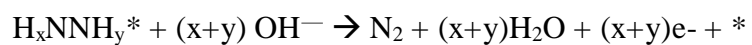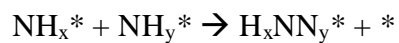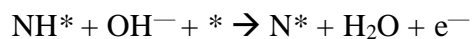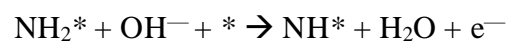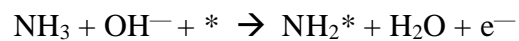
The main objective of this study is to determine the path of ammonia oxidation to N_2 on Pt (100) and explain why NH_3 oxidation is faster on Pt (100) than Pt (111).

Chapter 2

Methods

2.1 Electronic Structure Methods

Density functional theory was used to examine the electronic structure of surface intermediates and transition states along the ammonia oxidation path on Pt (100) and Pt (111) electrode surfaces. The Vienna ab initio simulation package (VASP) was used to perform electronic structure calculations employing a plane-wave basis set and the Perdew-Wang (PW91) exchange-correlation functional.[15-18] Ion core potentials were modeled by the projector augmented wave (PAW) approach[19,20] A 7 X 7 X 1 Monkhorst-Pack mesh was used to sample k-space for all surface cells.[21] The cutoff energy for the basis was 450 eV. Structural optimizations were completed when the magnitude of the forces on the atoms was less than 0.02 eV Å^{-1}. A convergence test with respect to the plane-wave cutoff energy and k-space sampling mesh was performed and all energies are converged within 0.003 eV. Dipole corrections along the surface normal direction were included (LDIPOL = TRUE, IDIPOL = 3). The experimentally measured Pt lattice constant of 3.92 Å was used.[22] All surface calculations utilized a 4-layer slab with the bottom two layers frozen to simulate the behavior of the bulk metal during optimization. The preferred adsorption site of each adsorbate was analyzed at 1/4 ML (in the 2 X 2 unit cell). Results testing preferred adsorption sites are given in Table 2 of the Supporting Information. On Pt (100) at ¼ ML, NH_3* prefers the atop site, NH_2* prefers the bridge site, NH* prefers the hollow site,

and N₂H₄* prefers the atop site with only one of the nitrogen atoms bound to the surface; images

are illustrated in Table 2.

DFT and statistical mechanics were used to examine the thermodynamics and kinetics of

the ammonia oxidation reaction on Pt (100). The free energy of formation of each adsorbed

intermediate on Pt (100) (relative to nitrogen gas at standard state) was calculated as a function of

potential. Equilibrium potentials, representing the potential at which formation of a particular

intermediate becomes favorable, were also calculated for select intermediates. Reaction kinetics

were investigated by using DFT to calculate transitions sites for nitrogen-nitrogen bond forming

reactions as well as for select proton transfer reactions.

2.2 Free Energy of Formation

The free energy of an adsorbed species X*, G_{X*}, is calculated as

$$G_{X*} = E_{X*}^{DFT} + ZPVE_{X*} - TS_{X*}^{vib}$$

(1)

The DFT energy of the adsorbed species is given as E_{X*}^{DFT}, the zero-point vibrational energy

as $ZPVE_{X*}$, and the vibrational entropy of the adsorbate as TS_{X*}^{vib}. It is assumed that the vibrational

entropy of the adsorbed species is the major contribution to entropy, and that the surface phonon

modes are not perturbed by adsorption. Therefore, the free energy of the bare surface is calculated

as Equation (2).

$$G_* = E_*^{DFT} \tag{2}$$

We reference adsorbate formation energies to $N_2(g)$. An example is below, Equation (3), where the subscripts x and y represent the stoichiometric coefficients, the number of protons on each nitrogen in the nitrogen containing adsorbates.

$$\Delta G_{H_xNNH_{y^*}} = G_{H_xNNH_{y^*}} - G_{N_2(g)} - (x+y)[G_{H^+_{aq}} + G_{electron}] - G_* \tag{3}$$

The free energy of the aqueous proton, $G_{H^+_{aq}}$, and electron pair is calculated using the computational hydrogen electrode:[37]

$$G_{H^+_{aq}} + G_{electron} = G_{H_2(gas)} - |e|U_{RHE} \tag{4}$$

where U_{RHE} is the electrode potential on a reversible hydrogen electrode scale.

2.3 Calculating Intermediate Formation Potentials with Coverage Dependence

We considered the coverage dependence of adsorption energies for a subset of adsorbed intermediates by varying the number of adsorbates in the unit cell. The equilibrium formation potential was then calculated for various coverages by plugging equation 4 into equation 3 and solving for the potential at which the formation free energy is 0. This gives the following equations for adsorption equilibrium potentials with X mono-nitrogen species (equation 5) or Y di-nitrogen species (equation 6) in the unit cell:

$$U^0_{RHE} = (XG_{H_2(gas)} - G_{XNH_{2^*}} + G_{N_2(g)} + G_*)/X \tag{5}$$

$$U^0_{RHE} = (2YG_{H_2(gas)} - G_{YN_2H_{4^*}} + G_{N_2(g)} + G_*)/2Y \tag{6}$$

2.4 Identifying Transition States and Activation Barriers

Transition states along minimum-energy paths for all N-N bond formation and select NH_x* deprotonation steps are located using the climbing image nudged elastic band method (CI-NEB).[23-26] Each reaction coordinate is discretized with either 6 or 10 images, including endpoints, with a tangent force criterion of less than 0.05 eV $Å^{-1}$ at the transition state and atomic forces on each adsorbate atom less than the same value. Each transition state was confirmed by vibrational frequency calculations, resulting in a single negative curvature mode. An example of a nitrogen-nitrogen bond formation barrier calculation is written as Equation (7) and a deprotonation barrier as Equation (8).

$$\Delta G^t_{H_y NNH_x*} = G_{TS} - G_{NH_x*+NH_y*} \tag{7}$$

$$\Delta G^t_{NH_x*+H*} = G_{TS} - G_{NH_{x+1}*} \tag{8}$$

ΔG^t is the activation energy to form species $X*$ and G_{TS} is the free energy of the transition state. The free energy of the reactant(s) is subtracted from G_{TS} to calculate ΔG^t.

Developing a DFT model to compute the barrier for proton transfer to solution is challenging. We modeled deprotonation as occurring via dehydrogenation to form a surface H atom. This method[27-28] assumes that the barrier of proton transfer to solution is equivalent to the deprotonation barrier at the potential where the free energy of the proton in solution is equal to that of adsorbed hydrogen. We also analyzed the proton transfer barrier by shuttling the hydrogen to the surface through an adsorbed water molecule. Since hydroxide adsorbs at potentials near the onset of ammonia oxidation on Pt (100), we also considered the barrier for proton transfer to an adsorbed hydroxide species adjacent to NH_x*.[30]

Chapter 3

Results and Discussion

We examine the mechanism for electrochemical oxidation of ammonia on Pt (100) and compared it to previously reported data on Pt (111). In section 3.1, we evaluate the full set of elementary electrochemical reaction energies for ammonia oxidation to nitrogen on the Pt (100) surface, with all adsorbates at ¼ ML coverage. In section 3.2, we report barriers for N-N formation at ¼ ML coverage. We then consider the coverage dependence of adsorption energy at preferred sites for key intermediates in section 3.3, followed by coverage dependence of activation barriers in section 3.4. All equilibrium and transition state structures located with DFT are illustrated in the Supplementary Information.

3.1 Overall NH₃ Oxidation Path at 1/4 ML Coverage

Figure 1 reports the DFT determined NH$_3$ oxidation free energy diagram on Pt (100) at 0.05 V$_{RHE}$ and all adsorbates at ¼ ML coverage. 0.05 V$_{RHE}$ is the nitrogen reduction to ammonia (NRR) equilibrium potential.[39] All NH$_x$ and H$_x$NNH$_y$ species were optimized to their lowest free energy state. These free energies are also tabulated in Supporting Information.

Mavrikakis et al. completed a similar DFT study of ammonia oxidation on Pt (111) (adsorbates at 1/9 ML coverage), and their reported energetics are reproduced in Figure 2.[13] Comparing the two surfaces, Pt (100) expresses a much stronger binding affinity for NH$_2$ (0.58 eV stronger). The large exergonic free energy for NH$_3$* to NH$_2$* on Pt (100) compared to Pt (111)

suggests that the rate of NH_2* formation is likely faster on Pt (100), and the rates of subsequent steps could be slower on Pt (100), assuming a BEP type relation holds. In addition to binding NH_2* stronger, Pt (100) also binds N_2H_4* stronger by 0.60 eV. NH*, however, binds somewhat more strongly to the (111) facet. Formation energies of these important intermediates are shown in Figure 2 for both Pt (100) and Pt (111). NH_2* and NH* are both candidates to participate in the proposed rate limiting step involving dimerization to form an N-N bond. [6, 10, 35] Significant differences in NH*, NH_2*, and N_2H_4*, stability between the facets are suggestive that substantial differences in ammonia oxidation rates may result, as observed experimentally.[6, 36]
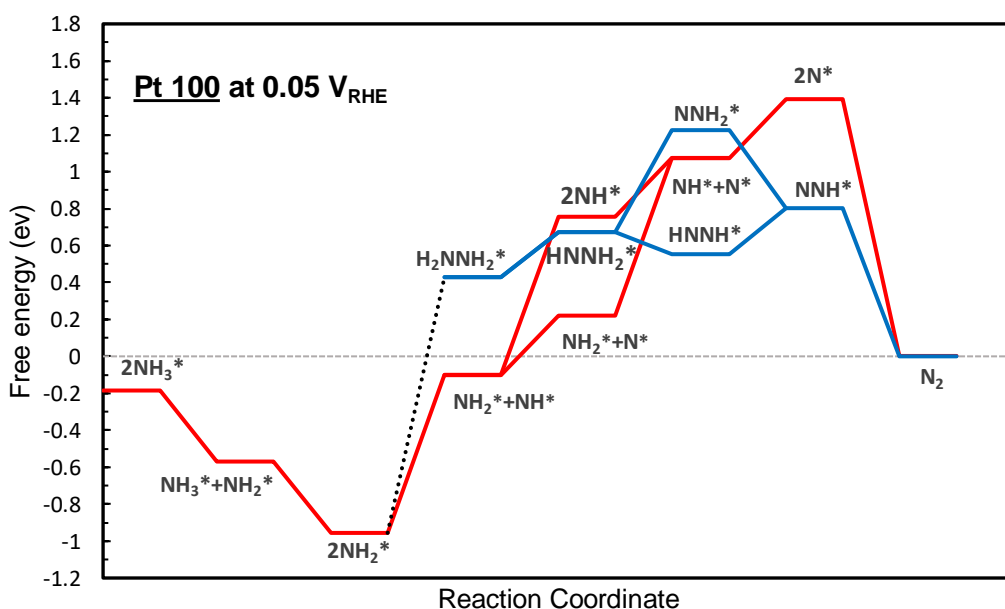

Figure 1. Free energy diagram of electrochemical ammonia oxidation on Pt (100) at 0.05 V_RHE. All energies are given with an adsorbate coverage of 1/4 ML. The free energies are calculated relative to N_2(g), the bare Pt surface, and the appropriate number of protons and electrons. N+N Mechanism is solid red, Gerischer-Mauerer mechanism is solid blue, and the dashed line is the proposed N-N bond formation step for both facets.
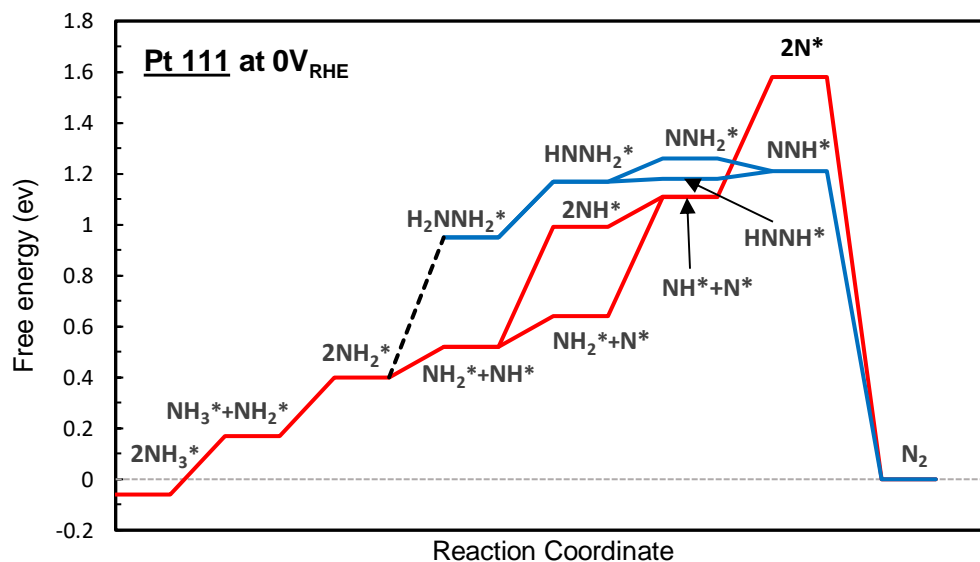
Figure 2. Free energy diagram of electrochemical ammonia oxidation on Pt (111) at 0 V$_{RHE}$. All energies are given with an adsorbate coverage of 1/4 ML. The free energies are calculated relative to N$_2$(g), the bare Pt surface, and the appropriate number of protons and electrons. In b.) all energies are given with adsorbates at a low adsorbate coverage of 1/9 ML.[13] N+N Mechanism is solid red, Gerischer-Mauerer mechanism is solid blue, and the dashed line is the proposed N-N bond formation step for both facets.
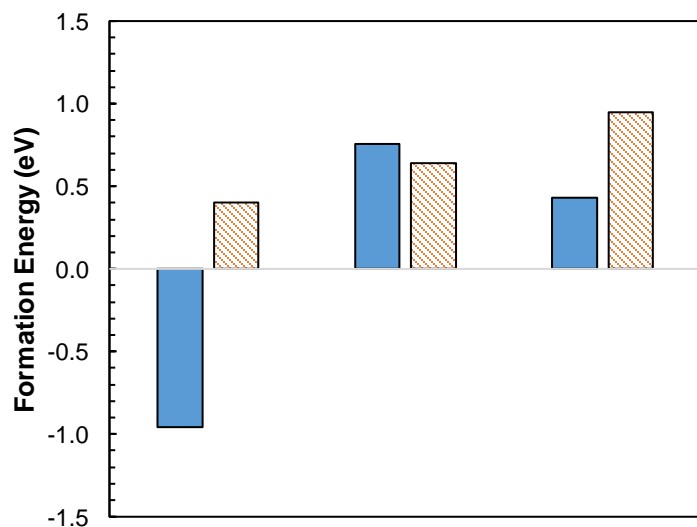
Figure 3. Formation energies (eV) of adsorbates at ¼ ML on both Pt (100) and Pt (111).[13] Pt (100) data is solid and blue. Pt (111) data is dashed and orange.

Reaction free energies suggest that, at low coverage, it is more favorable to adsorb NH_2* onto the surface of Pt (100) than Pt (111), but it is less favorable to dimerize on Pt(100). This is shown in Figure 4 with key elementary reaction energies. NH_2* formation is 0.6 eV more favorable on Pt (100), however NH_2* dimerization is 0.6 eV less favorable. As discussed in sections 3.3 and 3.4, the coverage dependence of these adsorption and reaction free energies must be examined before considering how these energetics impact NH_3 oxidation rates.
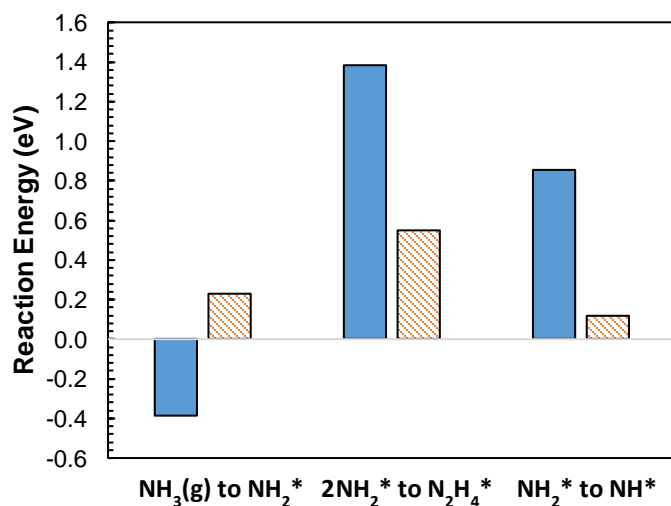
Figure 4. Elementary reaction energies at 0 V$_{RHE}$ of adsorbates at ¼ ML on Pt (100) and Pt (111). Pt (100) data is solid and blue. Pt (111) data is dashed and orange.

3.2 N-N Formation Barriers at Low Coverage

Activation barriers to form dinitrogen species are reported in Figure 5. Barriers were calculated at low coverage (1/4 ML) and compared to Pt (111) data reported by Mavrikakis et al. in which adsorbed species are at low coverage (1/9 ML). The low coverage data demonstrate that the strong adsorption of NH_2* on Pt (100) results in large barriers for reactions where NH_2* is a reactant. In contrast, the slightly stronger binding of N_2H* and N_2H_2* on Pt (100) than on Pt (111)

result in smaller barriers for reactions which form these intermediates, with the smallest barriers on Pt (100) coming from N-N bond formation between N^* and NH^* (~0.36 eV), as well as NH^* dimerization (~0.37 eV). This agrees with prior DFT data showing that NH_2^* dimerization is unfavorable due to a high kinetic barrier, and with increased electrode potential, the pathway favors N-N bond formation through NH^* dimerization.[8] However, the high stability of NH_2^* on Pt (100) may drive a higher coverage than considered here, as discussed in the next section.
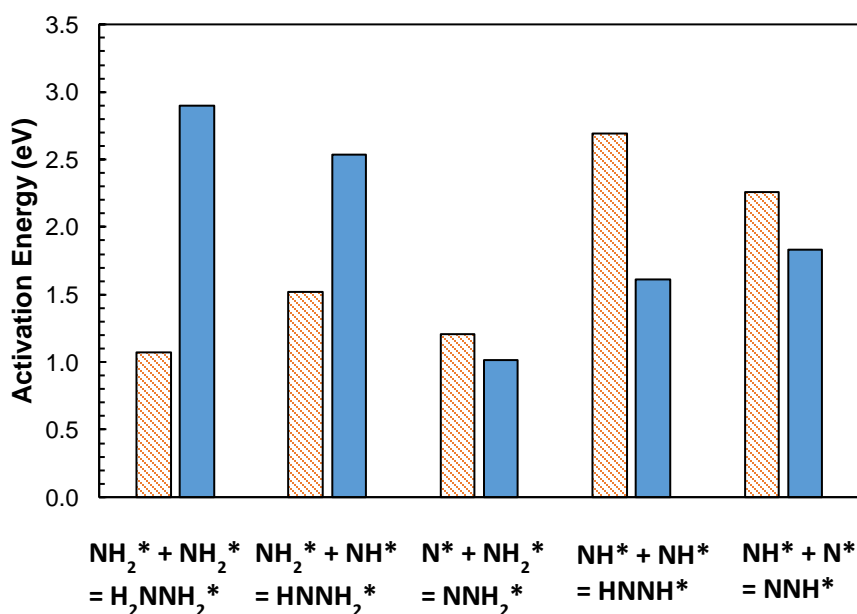
Figure 5. Low coverage barriers to from dinitrogen species from mono-nitrogen species on Pt (100) and Pt (111).[13] Pt (100) data is solid and blue. Pt (111) data is dashed and orange.

Figure 6 shows the initial, transition, and final state for NH_2^* dimerization on Pt(100). These structures will be contrasted to the high coverage NH_2^* dimerization structures in a later section. At low coverage, NH_2 dimerization requires significant rearrangement in which one of the NH_2^* species leaves its bridge-bound position to enable N-N bond formation, leading to a high activation barrier.
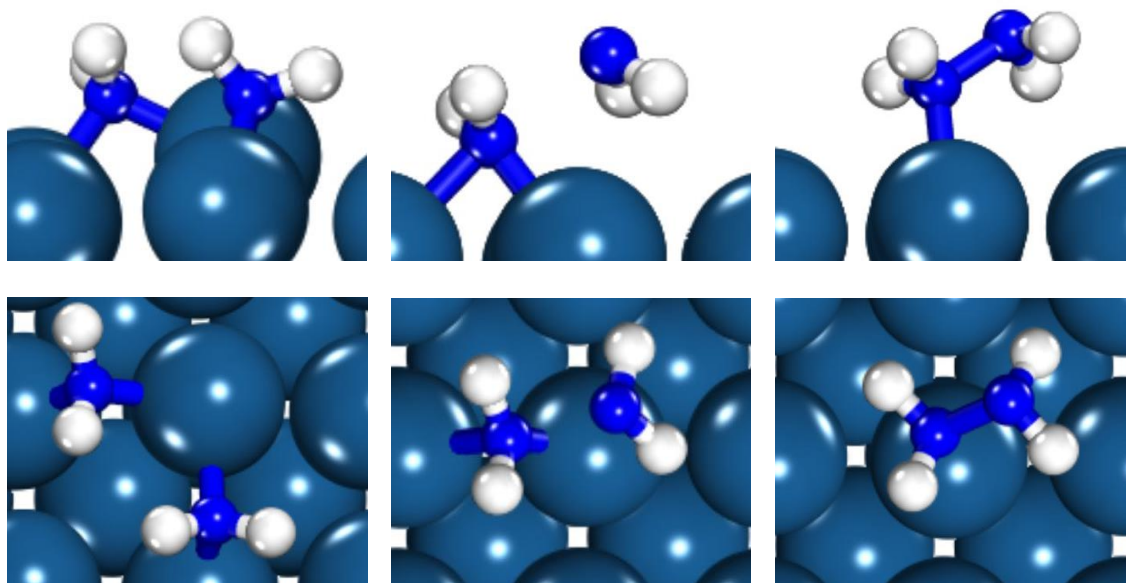
Figure 6. Transition state images (side and top views) of 2NH2* to N2H4* on Pt (100) with bridge site configuration for initial state. Pt atoms are shown in blue-grey, N atoms are shown in royal blue, and H atoms are shown in white.

3.3 Coverage Dependence

Due to the significantly more favorable formation energy and strong binding of NH_2* on Pt (100) relative to Pt (111), and its importance as an intermediate in the proposed rate-limiting steps in the ammonia oxidation reaction, we have examined the coverage dependence of formation of NH_2* on both Pt (100) and Pt (111). The coverage dependence of the equilibrium formation potential of NH_2* is significantly different on Pt (100) from Pt (111), shown in Figure 7. The atop adsorption trend of a slight increase in adsorption favorability with increased NH_2* coverage is similar on both facets. Adsorption on a bridge site is significantly stronger at low coverage on Pt (100) than on Pt (111), which agrees with a prior low coverage adsorption analysis.[10] Though low coverage NH_2* binds much more strongly on Pt (100), high coverage NH_2 is only 0.3 eV more stable on Pt (100) than on Pt (111). Both Pt (100) and Pt (111) coverage data shows a transition

from bridge NH_2* adsorption to atop NH_2* adsorption at high coverage. At high coverages, the atop configuration is more stable than the bridge site because neighboring NH_2* adsorbates hydrogen bond with each other, further justifying the suggestion made by Rosca and Koper that the formation of NH_2* adsorbates below *ca*. 0.5 V does not result in immediate dimerization of NH_2*, as more positive potentials are required to generate a sufficiently high NH_2* coverage.[10] This motivates examination of NH_2* adsorption in greater detail, looking into the coverage dependent kinetics of N_2H_4* formation.
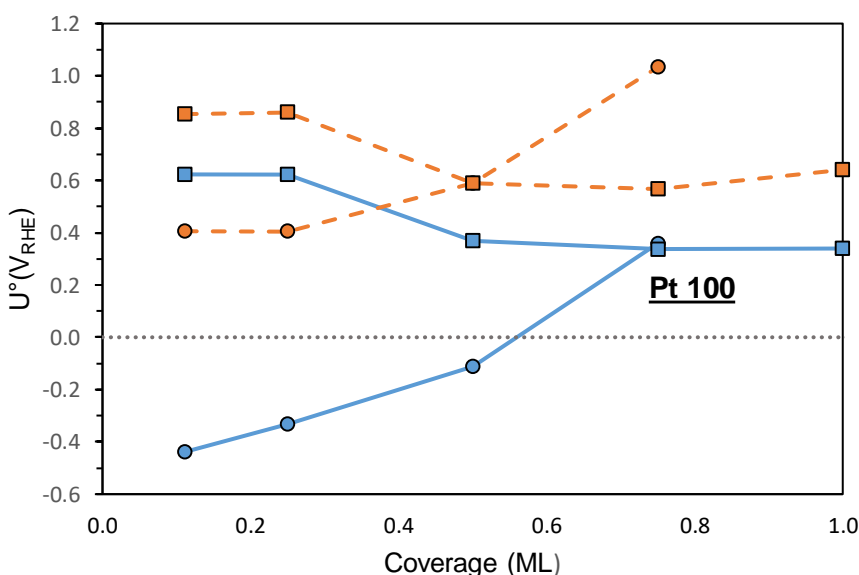
Figure 7. Equilibrium potential for the formation of NH_2* from NH_3 (g) as a function of adsorbate coverage on Pt (100) (blue solid lines) and Pt (111) (orange dashed lines) surfaces. The bridge and atop adsorption sites are shown at each coverage, with ● indicating the bridge sites and ■ indicating the atop sites.

Additional analysis of coverage dependence was completed for the NH* and N_2H_4* adsorbates on Pt (100), shown in Figure 8, to further compare our data with the reaction energetics at low coverage. With increased coverage, the formation energy of all species increases, except for atop NH_2*. NH* showed the largest increase in required formation energy (~1.7 eV from ¼ ML to 1 ML), suggesting that NH_2 dimerization will be more favorable than

deprotonation to NH* at high coverage. The small change in N_2H_4* formation energy (~0.4 eV from ¼ ML to ¾ ML) suggests that the competition between dimerization and deprotonation will favor N_2H_4* formation at high coverage.
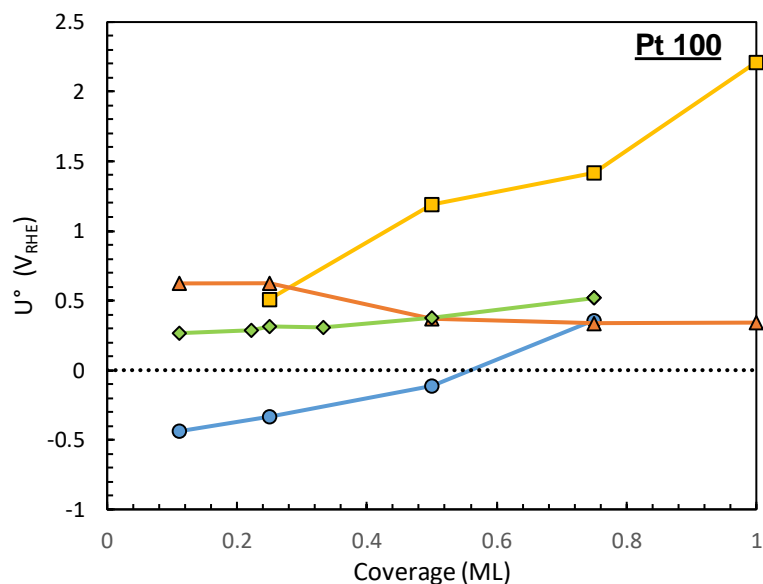
Figure 8. Equilibrium potential for the formation of key adsorbates on Pt (100) as a function of coverage: NH* (▪), NH_2* bridge (●), NH_2* atop (▲), and N_2H_4* (◆).

At high coverage, the formation of NH_2 on Pt (100) is still more favorable than on Pt (111). Figure 9 compares the reaction energies for the elementary steps between Pt (111) and Pt (100) surfaces at 1 ML coverage. 1 ML coverage of N_2H_4 is representative of 1 N_2H_4 per Pt atom since the most favorable position of N_2H_4 is atop with only one of the nitrogen atoms bound to the surface, as illustrated in Table 6 of the Supporting Information.
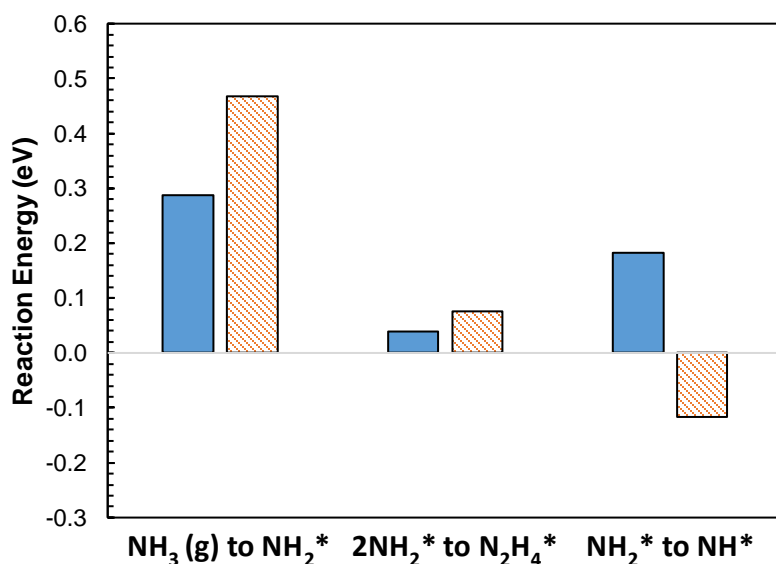
Figure 9. Elementary reaction energies of adsorbates at high coverage (1 ML) on Pt (100) and Pt (111) at 0.05 V_{RHE} and 0 V_{RHE}, respectively. Pt (100) data is solid and blue. Pt (111) data is dashed and orange.

3.4 N-N Formation Barriers at High Coverage

Table 1 presents the NH_2* dimerization barriers for both Pt (100) and Pt (111) surfaces at high coverage. Calculations were performed with 1 ML coverage to account for the buildup of NH_2* due to the rate-limiting nature of N_2H_4* formation on both surfaces.

Table 1. Activation barriers for NH_2* dimerization at high coverage (1 ML) for both Pt (100) and Pt (111) surfaces[13]

Surface	2 NH_2* to N_2H_4* Barrier
111	0.97 eV
100	0.30 eV

Based on both reaction energies and activation barriers, NH_2* dimerization is more favorable on Pt (100) than Pt (111). The lower barrier at high NH_2* coverage compared to low

NH$_2$* coverage on Pt (100) agrees with the more favorable reaction energy at high coverage. Figure 10 shows the initial state, transition state, and final state structures for NH$_2$* dimerization on Pt (100). The initial state has hydrogen bonding between NH$_2$* adsorbates. A hydrogen bond needs to be broken at the transition state, however, the significant rearrangement required for the low-coverage transition state in Figure 6 is not required when high-coverage NH$_2$ is bound at atop sites. High coverage, therefore, avoids the need to move NH$_2$* from strongly bound bridge sites and leads to the significant lowering of the dimerization activation barrier.
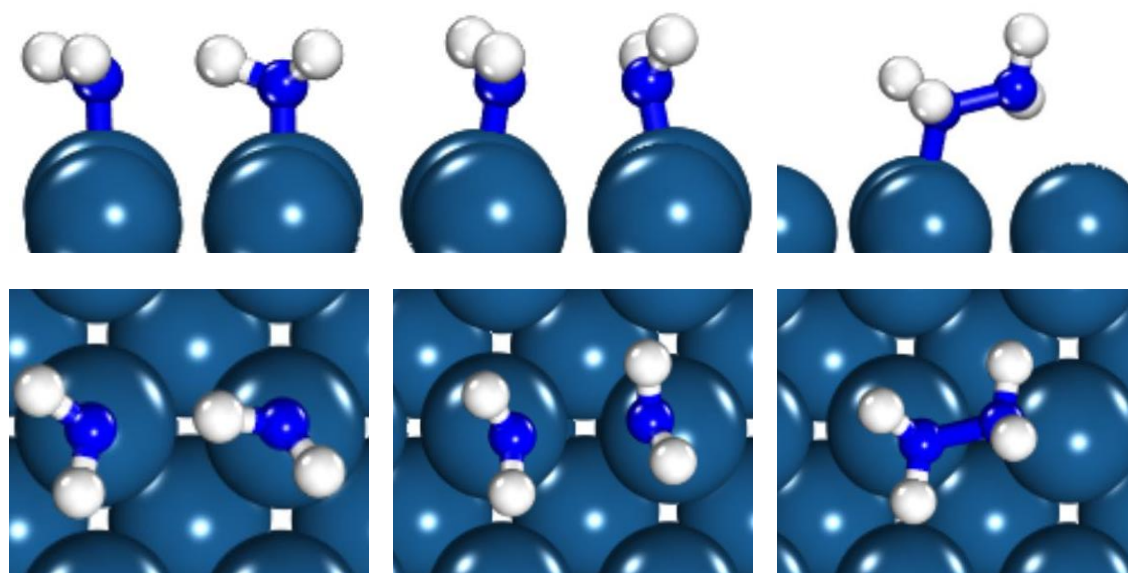
Figure 10. Transition state images (side and top views) of 2NH$_2$* to N$_2$H$_4$* on Pt (100) with atop site configuration for initial state. Pt atoms are shown in blue-grey, N atoms are shown in royal blue, and H atoms are shown in white.

The lowered barrier of NH$_2$* dimerization on Pt(100) with high coverage may account for the faster rate of NH$_3$ oxidation on this facet. We have assumed, however, that NH$_2$* dimerization is preferred over NH$_2$* oxidation to NH*. We have also assumed that dimerization is rate limiting, and therefore that NH$_3$* oxidation to form NH$_2$* occurs over a lower barrier than the dimerization

step. We computed electrode-potential dependent activation barriers for these steps to assess these assumptions.

NH$_2$* dehydrogenation is used to model the electrode potential dependent barrier for the equivalent electrochemical oxidation reaction via the method developed by Rostamikia et al.[27] Figure 11 compares the NH$_2$* dimerization barrier to that for the NH$_2$* oxidation to NH* plus a proton and an electron. Barriers are computed with and without water assistance during N-H dissociation, and with the presence of co-adsorbed hydroxide to accept the dissociating H species. Initial, transition, and final states used to model these steps are illustrated in Table 9 of the Supporting Information. Comparing the deprotonation barriers with the NH$_2$* dimerization barrier at low coverage, we would reach the same conclusion as Katsounaros et al.[14] that deprotonation is much faster than dimerization. When high coverage is considered, however, NH$_2$* deprotonation generally has a higher barrier than dimerization, suggesting NH$_2$* will dimerize before continuing along an oxidative path. At higher overpotentials and in the presence of co-adsorbed OH*, deprotonation may occur over lower barriers than dimerization. However, we note that deprotonation barriers were calculated at low coverage, and can be expected to increase with higher coverage of NH$_2$* due to the greater difficulty in breaking bonds with high coverage adsorbates. We also qualify that the method used to determine deprotonation barriers is approximate and sensitive to the number of water molecules included to represent solvation effects. Based on the presented results, we suggest that NH$_2$* dimerization will dominate over NH$_2$* oxidation, with the caveat that the conclusiveness of this result is limited by the difficulties in determining potential dependent barriers for electrochemical reactions and the lack of a full microkinetic analysis.
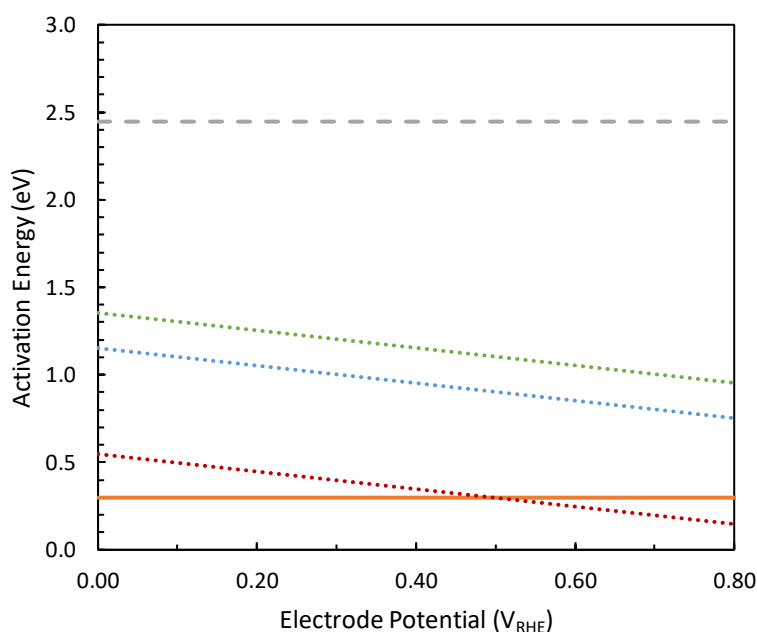
Figure 11. NH₂ dimerization activation barrier at high (flat solid orange line) and low (flat dashed line) coverages compared to NH₂ deprotonation barriers (dotted lines) as a function of electrode potential. NH₂* deprotonation barriers were determined with water-shuttling (green), no-shuttling (blue), and OH-shuttling (red) of the proton, in descending order.

The presence of surface adsorbed hydroxide provides the possibilty of a lower NH_2* deprotonation barrier than the NH_2* dimerization barrier at high coverage, however, the likelihood of hydroxide binding to the Pt (100) surface is low due to the strong adsorption potential of NH_2*. Additionally, the deprotonation barriers were calculated with NH_2* bridged between Pt (100) atoms, which is a charactersitic of low coverage NH_2* rather than high coverage. When compared to the NH_2* initial state at low coverage, it can be assumed that high coverage NH_2* would provide a less stable transition state for deprotonation because of the additional molecular shifting needed to achieve the the threefold configuration of the final state NH*, therefore increasing the overall NH_2* deprotonation barrier.

Our consideration of NH_2* dimerization at high coverage was motivated by high NH_2* stability and an assumption that NH_3* oxidation to NH_2* is significantly faster than NH_2*

dimerization. To validate this assumption, we calculated the activation barrier for NH_3^* dehydrogenation. Figure 12 considers the involvement of water and hydroxide within NH_3^* deprotonation. Hydroxide adsorbs at potentials near the onset of ammonia oxidation on Pt (100)[40, 41] and, therefore, could be present on the surface. The deprotonation mechanism of NH_3^* to NH_2^* involves the removal of a hydrogen atom through hydroxide shuttling, and this is significantly more favorable for NH_3^* deprotonation than without OH* co-adsorption. The formation of OH* at lower potentials on Pt(100) than Pt(111) may also contribute to the faster NH_3^* oxidation on the Pt(100) facet. Additionally, all deprotonation steps of $N_2H_4^*$ to $N_2(g)$ are fast, which agrees with experimental data of dehydrogenation reactions occurring at lower temperatures than dimerization on both Pt (100) and Pt (111).[38]
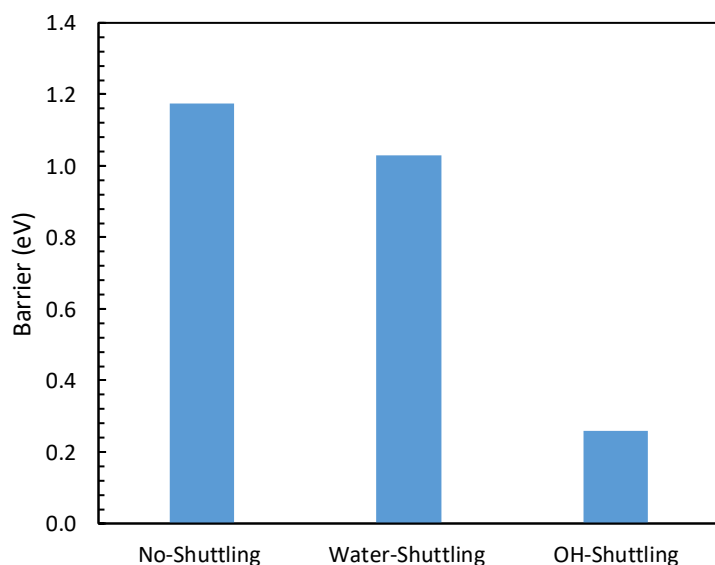
Figure 12. NH_3^* to NH_2^* + H^+ + e^- activation barriers at low coverage (1/4 ML) and 0.05 V_{RHE} for ammonia oxidation on Pt (100) using various deprotonation mechanisms.

Comparing energetics, Pt (100) will show faster NH_2^* dimerization due to lower barriers than on Pt(111) at high NH_2^* coverage. The step was proposed by Gerischer and Mauerer and further justified by Rosca and Koper as the rate limiting step; this lower barrier is likely the reason

of the faster NH_3 oxidation on Pt (100) versus Pt (111). Our calculated NH_3* to NH_2* barriers are larger than dimerization at low over potentials, though the presence of water and favorable formation of surface hydroxide on Pt (100) at low NRR overpotentials can accelerate NH_3* oxidation to NH_2*.

Chapter 4
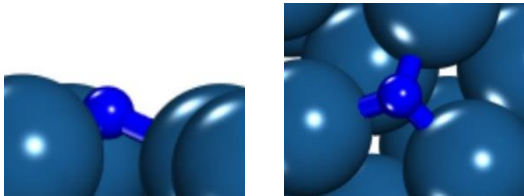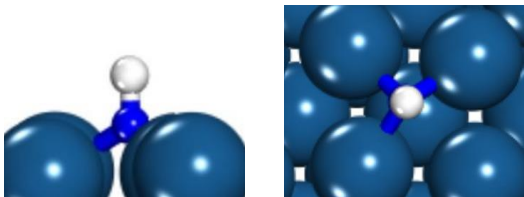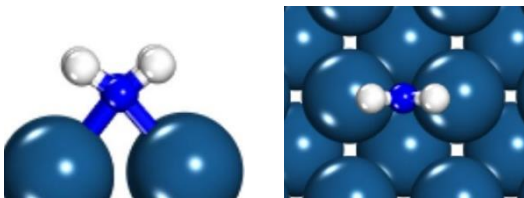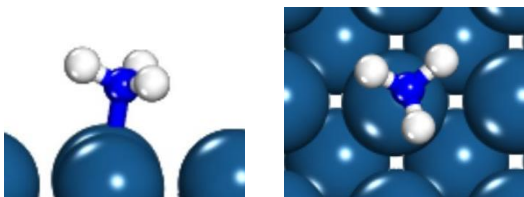
Summary and Conclusions
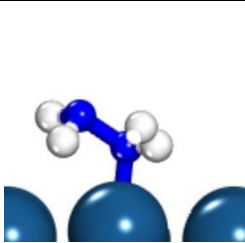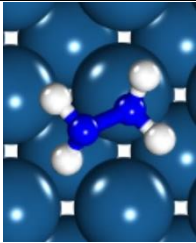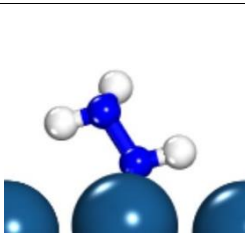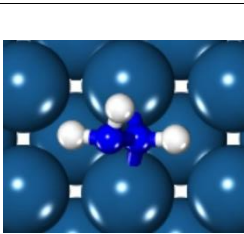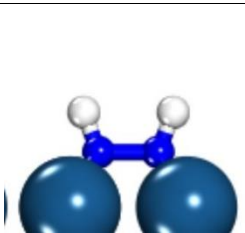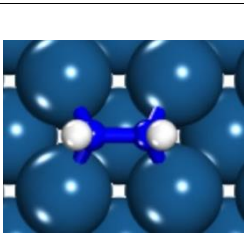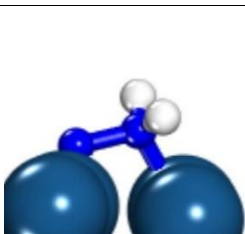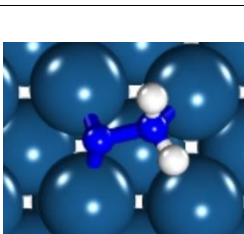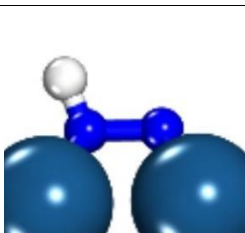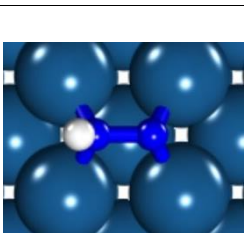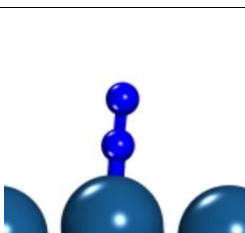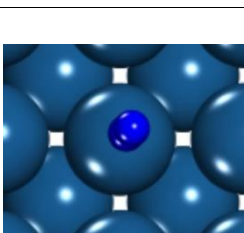
We studied the electro-oxidation of ammonia on the Pt (100) surface with density functional theory and compared our results to those previously reported in the literature.[13,14] Ammonia oxidation occurs via the Gerischer and Mauerer mechanism, with hydrogenated species forming the N-N bonds rather than complete deprotonation preceding N*-N* bond formation.

NH_2* is highly stable on Pt (100) and forms through rapid NH_3* deprotonation, assisted by water or co-adsorbed hydroxyl species. Greater NH_2* stability on Pt (100) compared to Pt (111) will lead to high NH_2* coverage. High coverage of NH_2* leads to a reduced N_2H_4* dimerization barrier that leads to more rapid NH_3 oxidation on Pt(100) in comparison to Pt(111).

Appendix A

Supporting Information

Table 2. Molecular images and energies for surface adsorbates on Pt (100)

Adsorbate	Image of Lowest Energy State	Energy (eV)
N*		-97.891
NH*		-101.934
NH$_2$*		-106.497
NH$_3$*		-110.290
N$_2$H$_4$*		-121.343

N$_2$H$_3$*		-117.590
HNNH*		-114.088
NNH$_2$*		-113.418
NNH*		-110.170
N$_2$*		-106.921
H$_2$*		-93.879
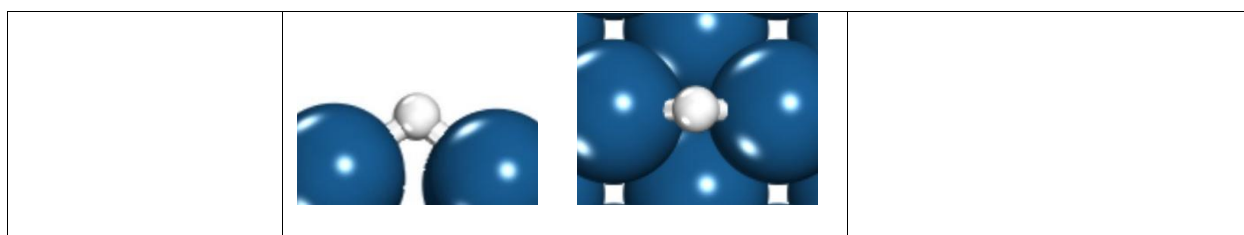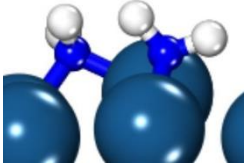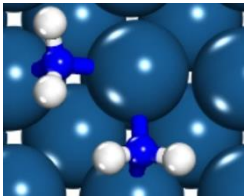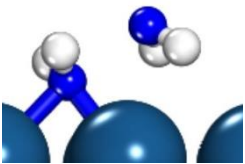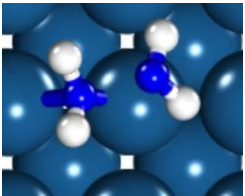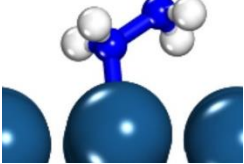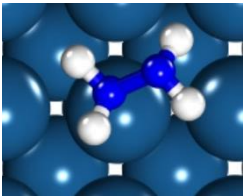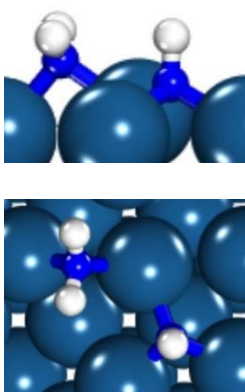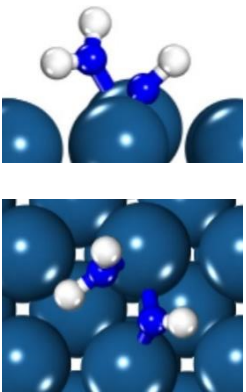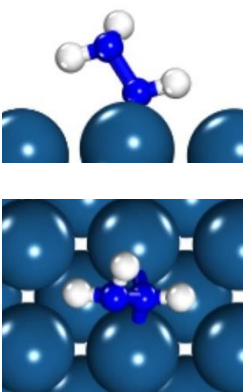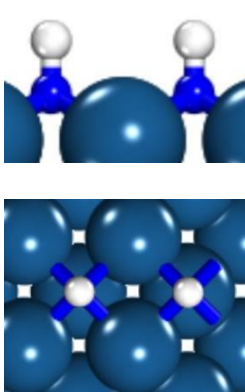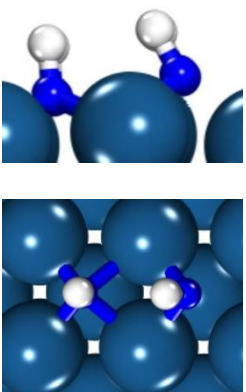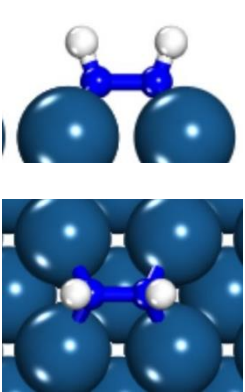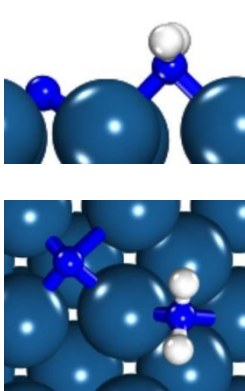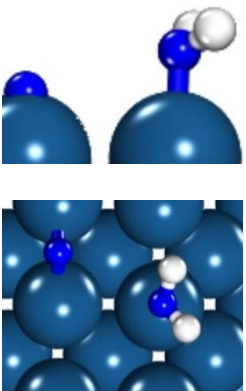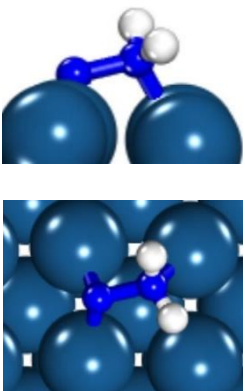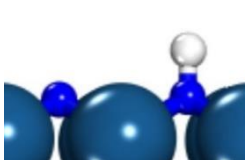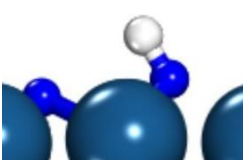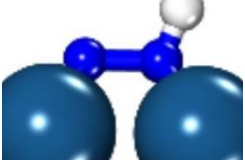
Table 3. The free energies of adsorbates calculated relative to N2(g), the bare Pt surface, and the appropriate number of protons and electrons entropy and vibration corrections.

Adsorbate	ΔG (eV)
$2NH_3*$	-0.18
$NH_3* + NH_2*$	-0.57
$2NH_2*$	-0.96
$NH_2* + NH*$	-0.10
$2NH*$	0.76
$NH* + N*$	1.07
$2N*$	1.39
N_2H_4*	0.43
N_2H_3*	0.68
$HNNH*$	0.55
NNH_2*	1.22
$NNH*$	0.80
N_2 (g)	0.00

Table 4. Molecular Images for low-coverage barriers on Pt (100)

Barrier	Initial State	Transition State	Final State
$NH_2* + NH_2* \rightarrow N_2H_4*$			

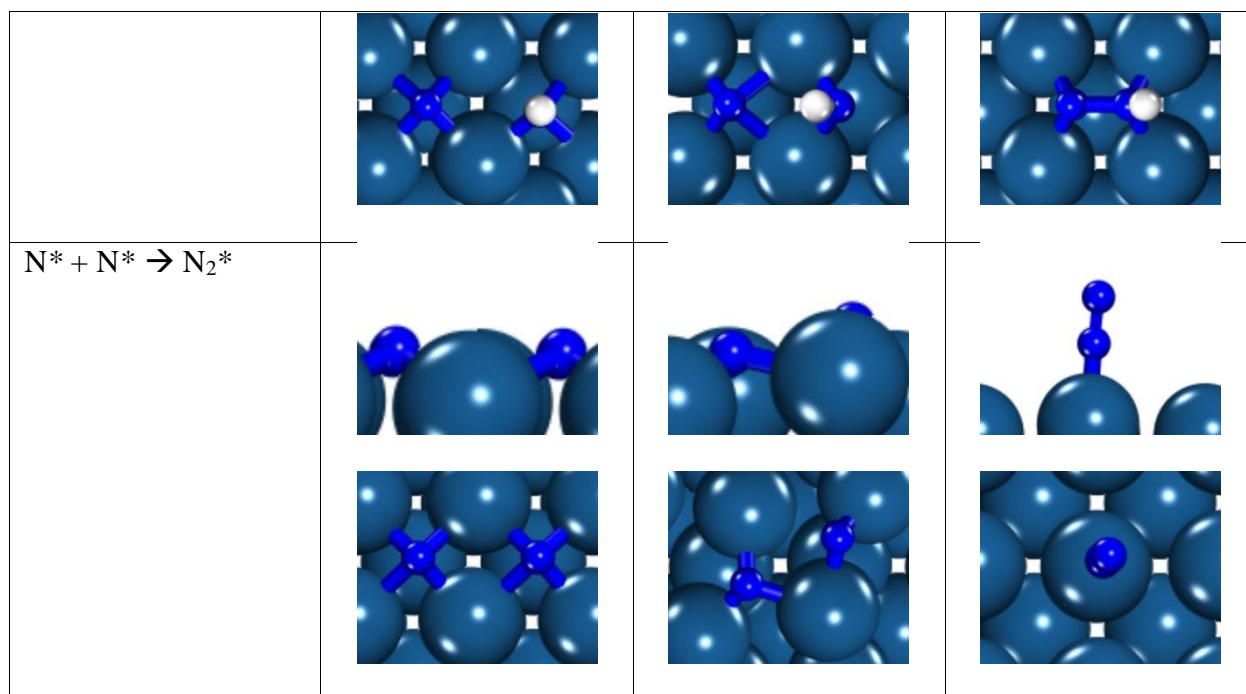|			
NH$_2$* + NH* → N$_2$H$_3$*			
NH* + NH* → HNNH*			
NH$_2$* + N* → NNH$_2$*			
NH* + N* → NNH*			
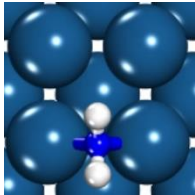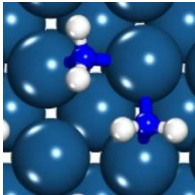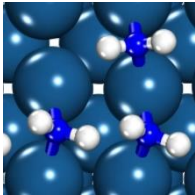
Table 5. Low coverage barrier calculations for N-N bond formation on Pt (100)

Barrier	ΔG^t (eV)
NH_2* + NH_2* → N_2H_4*	2.90
NH_2* + NH* → N_2H_3*	2.54
NH* + NH* → $HNNH$*	1.02
NH_2* + N* → NNH_2*	1.61
NH* + N* → NNH*	1.83

Table 6. Molecular images for coverage dependence on Pt (100) and Pt (111) in a 2x2 unit cell

Surface Adsorbate	1/4 ML	1/2 ML	3/4 ML	1 ML
Bridge NH_2* Pt (100)				Did not converge.
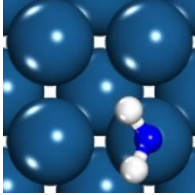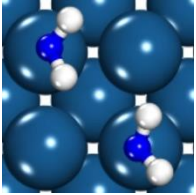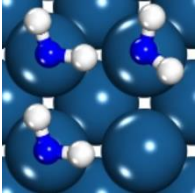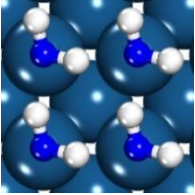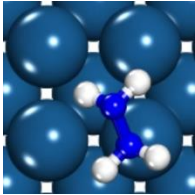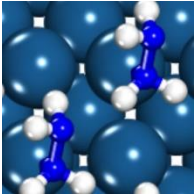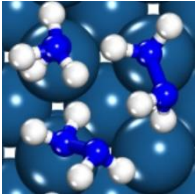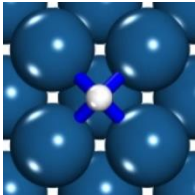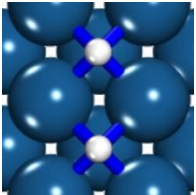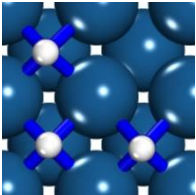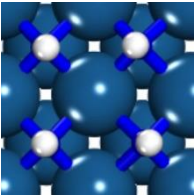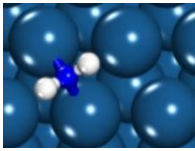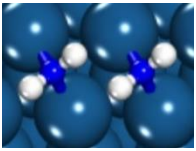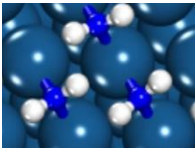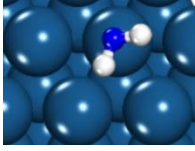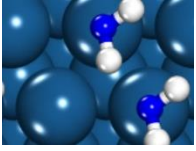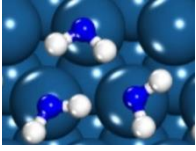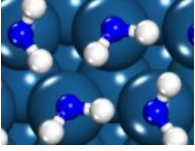
Atop NH$_2$* Pt (100)			
N$_2$H$_4$*			Did not converge.
NH*			
Bridge NH$_2$* Pt (111)			Did not converge.
Atop NH$_2$* Pt (111)			

Table 7. Equilibrium potential for adsorbates at varying coverage on Pt (100) and Pt (111)

Surface Adsorbate	U° (V_{RHE}) 1/4 ML	U° (V_{RHE}) 1/2 ML	U° (V_{RHE}) 3/4 ML	U° (V_{RHE}) 1 ML
Bridge NH$_2$* Pt (100)	-0.33	-0.11	0.36	Did not converge.
Atop NH$_2$* Pt (100)	0.62	0.37	0.34	0.34
N$_2$H$_4$*	0.27	0.28	0.30	Did not converge.

NH*	0.51	1.19	1.42	2.21
Bridge NH$_2$* Pt (111)	0.40	0.59	1.03	Did not converge.
Atop NH$_2$* Pt (111)	0.86	0.59	0.57	0.64

Table 8. Molecular images for high coverage barriers on Pt (100)
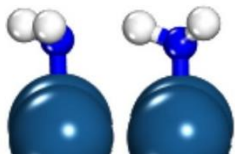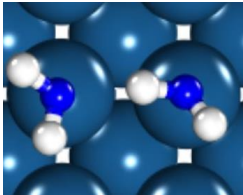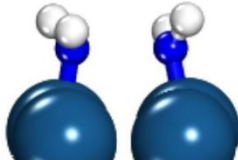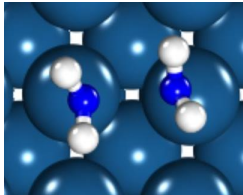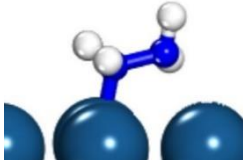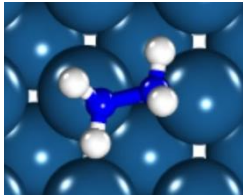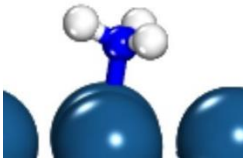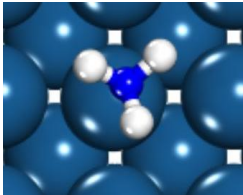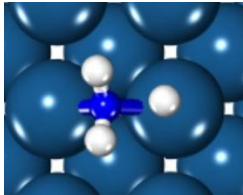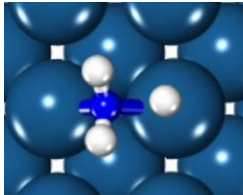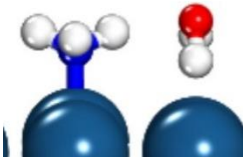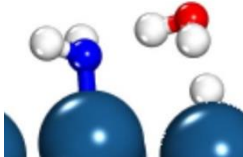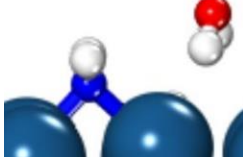
Barrier	Initial State	Transition State	Final State
NH$_2$* + NH$_2$* → N$_2$H$_4$*			

Table 9. Molecular images for deprotonation barriers on Pt (100)

Barrier	Initial State	Transition State	Final State
NH$_3$* → NH$_2$* + H*			
NH$_3$* + H$_2$O* → NH$_2$* + H$_2$O* + H*			

NH$_3$* + OH* → NH$_2$* + H$_2$O*			
NH$_2$* → NH* + H*			
NH$_2$* + H$_2$O* → NH* + H$_2$O* + H*			

NH$_2$* + OH* → NH* + H$_2$O*			

Table 10. Deprotonation barrier calculations on Pt (100)

Barrier	ΔG^t (eV)
NH$_3$* → NH$_2$* + H*	1.17
NH$_3$* + H$_2$O* → NH$_2$* + H$_2$O* + H*	1.03
NH$_3$* + OH* → NH$_2$* + H$_2$O*	0.26
NH$_2$* → NH* + H*	1.15
NH$_2$* + H$_2$O* → NH* + H$_2$O* + H*	1.35
NH$_2$* + OH* → NH* + H$_2$O*	0.55

BIBLIOGRAPHY

1. P. H. Pfromm, *J. Renew. Sustain. Energy*, 2017, **9 (3)**, 034702.

2. W. M. Stewart, A. E. Dibb, A. E. Johnston, and T. J. Smyth, *Agron. J.*, 2005, **97(1)**, 1–6.

3. R. Naylor, H. Steinfeld, W. Falcon, J. Galloway, V. Smil, E. Bradford, J. Alder, H. Mooney, and M. A. Sutton, *Science*, 2005, *310* **(5754)**, 1621–1622.

4. C. Feng, N. Sugiura, S. Shimada, and T. Maekawa, *J. Hazard. Mater.*, 2003, *103*, 65−78.

5. S. E. Jorgensen, *Pergamon Press*, 1975; **Vol. 9**.

6. A. Aldaz, F. J. Vidal-Iglesias, N. Garcıa-Araez, V. Montiel, and J. M. Feliu, *Electro. Comm.*, 2003, **5 (1)**, 22-26.

7. T. Pignet, and L. D. Schmidt, *Chem. Eng. Sci.* 1974, *29* **(5)**, 1123–1131.

8. T. H. Chilton, *M.I.T. Press*, 1968.

9. W. Offermans, A. Jansen, and R. V. Santen, *Surface Science*, 2006, **600 (9)**, 1714–1734.

10. V. Rosca, and M. Koper, *Phys. Chem. Chem. Phys.*, 2006, **8 (21)***,* 2513-24.

11. J. K. Nørskov, T. Bligaard, J. Rossmeisl, and C. H. Christensen, *Nat. Chem.*, 2009, **1**, 37−46.

12. J. Greeley, T. F. Jaramillo, J. Bonde, I. B. Chorkendorff, and J. K. Norskov, *Nat. Mater.*, 2006, **5**, 909−913.

13. M. Mavrikakis, P. Ferrin, and J. Herron, J, *J. Chem. Phys.*, 2015, **119 (26)**, 14692–14701.

14. I. Katsounaros, M. C. Figueiredo, F. Calle-Vallejo, H. Li, A. A. Gewirth, N. M. Markovic, and M. T. Koper, *J. Cat.*, 2018, **359**, 82–91.

15. G. Kresse, and J. Furthmeller, *Phys. Rev. B*, 1996, **54**, 11169 – 11186.

16. G. Kresse, and J. Furthmeller, Comput. *Mater. Sci.* 1996, **6**, 15 – 50.

17. G. Kresse, and J. Hafner, *Phys. Rev. B*, 1993, *47*, 558 – 561.

18. J. P. Perdew, J. A. Chevary, S. H. Vosko, K. A. Jackson, M. R. Pederson, D. J. Singh, and C. Fiolhais, *Phys. Rev. B.*, 1992, **46**, 6671 – 6687.

19. P. E. Blöchl, *Phys. Rev. B.*, 1994, **50**, 17953−17979.

20. G. Kresse, and D. Joubert, *Phys. Rev. B*, 1999, **59**, 1758.

21. H. J. Monkhorst, and J. D. Pack, *Phys. Rev. B*, 1976, **13**, 5188−5192.

22. C. Kittel, *J. Wiley*, 2008, **7**.

23. A. Ulitsky, and R. Elber*, J. Chem. Phys.*, 1990, **92**, 1510.

24. G. Mills, H. Jónsson, and G. K. Schenter, *Surf. Sci*, 1995, **324**, 305.

25. G. Henkelman, B. P. Uberuaga, and H. Jónsson, *J. Chem. Phys.*, 2000, *113*, 9901.

26. H. Jónsson, G. Mills, K. W. Jacobsen, B. J. Berne, G. Ciccotti, and D. F. Coker, *World Scientific*, 1998, p. 385.

27. G. Rostamikia, A. J. Mendoza, M. A. Hickner, and M. J. Janik, *J. Power Sources*, 2011, **196***, 9228-9237.

28. S. A. Akhade, N. J. Bernstein, M. R. Esopi, M. J. Regula, and M. J. Janik. *Catalysis Today*, 2017, **288** 63-73.

29. I. T. McCrum, S. A. Akhade, and M. J. Janik, *Electrochim. Acta* , 2015, **173**, 302–309.

30. R. Gomez, J. M. Orts, B. Alvarez-Ruiz, and J. M. Feliu, *J. Phys. Chem. B*, 2004, **108**, 228−238.

31. F. J. Vidal-Iglesias, J. Solla-Gullon, V. Montiel, J. M. Feliu, and A. Aldaz, *J. Power Sources*, 2007, **171**, 448−456.

32. C. Zhong, W. B. Hu, and Y. F. Cheng, *Mater. Chem. A*, 2013, **1**, 3216−3238.

33. H. Gerischer, and A. Mauerer, A. *J. Electroanal. Chem.*, 1970, **25**, 421−433.

34. K. Eguchi, T. Matsui, S. Shohei Suzuki, Y. Katayama, K. Yamauchi, T. Okanishi, and H. Muroyama, *Langmuir*, 2015, **31 (42)**, 11717-11722.

35. D. Skachkov, C. V. Rao, and Y. Ishikawa, *J. Phys. Chem. C*, 2013, **117**, 25451−25466.

36. F. J. Vidal-Iglesias, J. Solla-Gullon, A. Aldaz, V. Montiel, and J. M. Feliu J.M, *J. Phys. Chem. B*, 2005, **109**, 12914-12919.

37. J. K. Nørskov, J. Rossmeisl, A. Logadottir, L. Lindqvist, J. R. Kitchin, T. Bligaard, and H. Jonsson, *J. Phys. Chem. B*, 2004, **108**, 17886−17892.

38. A. C. A. De Vooys, M. T. M. Koper, R. A. Van Santen, and J. A. R. Van Vee. J. A. R, *J. Electroanal. Chem*., 2001, **506**, 127.

39. M. Nazemi, and M. A. El-Sayed, *J. Phys. Chem. Lett*., 2018, **9 (17)**, 5160–5166.

40. N. Garcia-Araez, V. Climent, and J. M. Feliu, *J. Electroanal. Chem.* 2010, **649**, 69−82.

41. I. T. McCrum, and M. J. Janik, *J. Phys. Chem C*, 2016, **120**, 457-471.

Academic Vita of Spencer Wallace

swwallace523@gmail.com

EDUCATION

2015-2019 | **The Pennsylvania State University,** *Schreyer Honors College – University Park, PA*
B.S. in Chemical Engineering, Minors in Energy Engineering and Environmental Engineering
Relevant Courses: Mass Transfer, Physical Chemistry, Fluid Mechanics, Thermodynamics, Biotechnology, Heat Transfer, Reaction Engineering, Polymer Science

WORK EXPERIENCE

May 2018-
August 2018

Engineering Technical Intern – Polypropylene
ExxonMobil – Baytown Chemical Plant , Texas
- Scoped a capital project to increase reactor cooling capacity with credits of $1.5M/year
- Led multiple plant tests to optimize catalyst-use and additive reliability saving $300K/year
- Designed facilities to instill a more robust pump flushing system to allow for better startup

August 2017-
December 2017

Engineering Technical Co-op – Olefins
ExxonMobil – Baytown Olefins Plant, Texas
- Simulated cold box processes and found a possible $500K/year profitable optimization
- Developed an SRV analysis for the ethane recycle unit within the main-train cold box
- Headed a 4-day catalyst change-out of an acetylene reactor

May 2017-
August 2017

Process Engineer Intern
PPG Industries – Carrollton, Texas
- Designed a system to automatically deliver potassium hydroxide as a pH buffer to architectural coatings to combat the 10+ chemical burn incidents per year

August 2017-
May 2018

Material Balances (Spring '18) and Thermodynamics II (Fall '18) Instructional Aide
Penn State University – Associate Proffesor Dr. Stephanie Velegol – University Park, Pennsylvania
- Held weekly office hours to help students better understand chemical engineering concepts
- Provided insight into teaching material balance and thermodynamic fundamentals

RESEARCH EXPERIENCE

August 2015- Present	**Chemical Engineering Undergraduate Researcher** *Research Director: Dr. Michael Janik – University Park, Pennsylvania* - Worked in Dr. Janik's research lab while taking part in a Summer 2016 REU - Modeled the electrocatalytic oxidation of ammonia on platinum using DFT

SERVICE AND ACTIVITIES

March 2017- Present	**Engineering Ambassadors** - Hosted 2 or more science stimulating events for young children each month - Led tours and recruiting events for the College of Engineering
October 2017- Present	**Schreyer Honors Career Development Program Mentor** - Mentored and guided three first year chemical engineering students
August 2015- Present	**THON Organization—Apollo** - Functioned as the 2018-2019 Member Relations Executive Chair - Served as the 2016-2017 Co- Donor and Alumni Relations Executive Chair - Danced at THON 2018 for the Lynch, Mummert, Sanchez, and Del Franco families
August 2015- Present	**Schreyer Honors College Student Orientation** - Coordinated the 300 person SHC class of 2022 orientation as an orientation leader - Assimilated 12 first year Schreyer students into Penn State as a 2016-2017 mentor

SKILLS

Proficient in: PRO II, Pegasys, Microsoft Office, Microsoft Publisher, Unix, Vienna Ab initio simulation package (VASP), Microsoft Excel, Mathematica, Photoshop Lightroom